Theoretical Calculation of Characteristic Radiation: Multiconfiguration Dirac-Hartree-Fock Calculations in Scandium $K\alpha$ and $K\beta$

Dean JW,* Pushkarna P, Melia HA, Nguyen TVB, and Chantler CT†
The University of Melbourne

The characteristic X-ray spectra of $3d$ transition metals are a constant source of advances in atomic physics, X-ray spectrometry, and quantum mechanics. Prior to this work, there was a discrepancy of 0.549 eV between theoretical and experimental results for the scandium $K\alpha_1$ peak energy, representing a 55σ discrepancy using the experimental uncertainty. This work improves this to a 0.330 eV discrepancy with only a 4σ error between experiment and theory. Furthermore, we add considerable evidence that asymmetries in X-ray spectra are described by shake events. This work provides *ab initio* calculations for the diagram and shake-off satellite lines of Sc $K\alpha$ and $K\beta$ and makes significant improvement on the previous fitting between theory and experiment, from a χ^2_r of 7.35 and 20.85 to 1.60 and 1.45 for $K\alpha$ and $K\beta$, respectively. Therefore, we make a strong claim that the asymmetries in scandium x-ray lines exist due to satellite lines with very little room for other hypothesised phenomena to exist, such as Kondo-like interactions and Doniac-Sunjic asymmetries. By fitting to the best experimental data for Sc $K\alpha, \beta$ we obtain values for the width and intensity of the satellite lines which enable us to reconstruct the $K\alpha$, $K\beta$ profiles.

INTRODUCTION

Atomic photo-emission lines arising from bound-bound electron transitions offered the first insight into atomic structure and quantum mechanics. Over one-hundred years later, the same phenomena are still at the forefront of research. The most widely used X-ray emission lines are the $K\alpha$ and $K\beta$ transitions arising from the $1s^{-1} \rightarrow 2p^{-1}$ and $1s^{-1} \rightarrow 3p^{-1}$ transitions respectively. The eigenvalue spectra of these transitions: offer insight into fundamental atomic processes; test advanced relativistic quantum mechanics and QED; and offer a range of practical applications such as medical [1], laser [2], fusion science [3], and many areas of astrophysics such as understanding binary systems [4, 5], probing galactic variabilities [6], and black hole spin [7]. in particular, X-ray free electron laser (XFEL) studies increasingly depend upon ad hoc empirical energy measurements in the absence of high accuracy theoretical or experimental values.

Since understanding these spectra is important to so many fields of science, it is striking that there exist major discrepancies between experimental and theoretical values in the literature. There is no better example than scandium $K\alpha^0_{1,2}$ and $K\beta^0$. The superscript, 0, indicates the reconstructed peak energy defined by the peak of the profile with zero Gaussian broadening. Hence this measure is a strong attempt at an optic-independent transferable parameter. Scandium $K\alpha^0_{1,2}$ and $K\beta^0$ theoretical (Deslattes et al. [8]) and experimental (Dean et al. [9, 10]) values differ by approximately 50σ for the three values, using the experimental uncertainty of 0.01 eV.

Such discrepancies are a strong motivation for current studies in atomic X-ray lines. Further, asymmetries in these spectra were first noted by Siegbahn and Stenstrom in 1916 [11], and over a hundred years later, lively debate continues regarding the mechanism by which these asymmetries arise.

Both of these issues owe much to the historic difficulty of atomic and quantum physics in a relativistic framework. Until recently it has been standard to treat relativistic effects as minor corrections to be made to Schrödinger equation solutions of atomic and molecular structures. Yet clearly, a fully relativistic quantum approach is necessary to marry theoretical and experimental energy values and resolve issues of asymmetries.

There are several attempts at understanding asymmetries in photo-emission spectra, these include exchange interactions [12], plasmon excitations [13], Kondo-like interactions [14], double electron transitions [15], and asymmetries due to multiple energy eigenvalues [16, 17]. The most common explanation, and indeed the focus of this work, are shake effects, or double ionisations, first suggested by Wentzel in 1921 [18, 19].

A shake event is when a second electron is excited, or *shaken*, from the atom into the continuum (shake-off) or into a higher shell (shake-up) during the ionisation of the core electron. We do not consider shake-up in this work since it is negligible compared to shake-off for the accuracies, which we will show later. The transition then takes place under a different potential to the main *diagram* line, giving different energy eigenvalues for these *satellite* lines. For example, the Kα $3d$ shake-off satellite line is $[1s3d]^{-1} \rightarrow [2p3d]^{-1}$.

Copper is the most well studied of the $3d$ transition metals, yet due to a lack of high accuracy *ab initio* calculations to compare with high resolution experiments the genesis of satellite lines remains an open problem. However, recent advances with copper calculations strongly suggest that shake events are necessary and dominant [20, 21]. There is a dearth of information in the literature on the other $3d$ transition metals. This is typified by scandium which has only one previous *ab initio* calculation of the $K\alpha$, $K\beta$ transitions with shake events

considered by Anagnostopoulos et al. [22]. There is another mention of these calculations in 2003 ([8] Table V, page 48); however, they reference an unpublished work by Anagnostopoulos, Indelicato, Gotta, and Simons which is yet to be peer reviewed. Certainly, part of the reason for the dearth of scandium calculations is due to the difficulties of its open shell electron structure, discussed below.

Ref. [22] is over two-decades old and with the advances in computational power, theoretical software packages, and experimental data with which to compare, there is a need for a new theoretical calculation. Furthermore, we expand on the prior calculation of scandium $K\alpha$, $K\beta$ spectra to include the $3s$ satellite line. This investigation is essential for increasing the understanding of complex atomic processes, testing state-of-the-art relativistic quantum mechanics, and supporting practical applications where X-ray fluorescence of scandium is involved.

THEORY

For this investigation we implement our theoretical model with a modified GRASP2K package which incorporates QED theory developed by Lowe et al. [23] and Breit interactions [24, 25]. The GRASP2K interactive software performs relativistic atomic structure calculations with the multi-configuration Dirac-Hartree-Fock (MCDHF) method [26–28]. In this section we discuss the theoretical framework on which the GRASP2K software is based. The next section provides more information on the specifics in implementing GRASP2K.

MCDHF is based upon the Dirac-Hatree-Fock (DHF) approach for many-electron systems where the atomic state functions (ASFs) are linear combinations of configuration-state-functions (CSFs):

$$\Psi(\Pi JM) = \sum_r c_r \Phi(\gamma_r \Pi JM) \tag{1}$$

where the CSFs, $\Phi(\gamma_r \Pi JM)$, are linear combinations of Slater determinant solutions to the central field problem obtained from orthornomalised spinors with well-defined parity, Π, angular momenta, JM, and all quantum numbers necessary for a unique electron configuration, γ_r. The coefficients, c_r, are found from diagonalising the Dirac-Coulomb Hamiltonian, H_{DC}:

$$H_{DC} = \sum_i^N (c\vec{\alpha_i} \cdot \vec{p_i} + V_{nuc.}(r_i) + (\beta_i - 1)c^2) + \sum_{i \geq j} \frac{1}{r_{ij}} \tag{2}$$

For an N-electron system, the full CSF is built from products of Dirac central field orbitals:

$$\Phi_{E\kappa m}(\vec{r}) = \mathcal{A}\Big[\prod_{i=1}^{N} \phi_{iE\kappa m}(\vec{r})\Big] \tag{3}$$

with:

$$\phi(\vec{r}) = \frac{1}{r} \begin{pmatrix} P_{E\kappa}(r)\chi_{\kappa m}(\theta,\varphi) \\ iQ_{E\kappa}(r)\chi_{-\kappa m}(\theta,\varphi) \end{pmatrix} \tag{4}$$

where the two-component spin-orbit functions $\chi_{\kappa m}(\theta,\varphi)$ include an amplitude and are simultaneously eigenfunctions of $\boldsymbol{j}^2$, $\boldsymbol{l}^2$, and $\boldsymbol{s}^2$, as well as being orthonormal. $\mathcal{A}$ is the antisymmetrisation operator, and $P_{E\kappa}$ and $Q_{E\kappa}$ are the large and small components of the radial wavefunction.

Often, first-order CSFs give good approximations to the full ASF (typically within 1%). First-order CFSs arise from the electron configuration ground states before and after transition and allowing for all possible electron j numbers. For scandium $K\alpha$ this would be the transition $1s^{-1} \rightarrow 2p^{-1}$ and j numbers $1 \rightarrow \{0, 2\}$, and $2 \rightarrow \{1, 3\}$ (four CSFs in total). A more complete calculation can be done when higher-order CSFs are considered.

Second-order and third-order CSFs are generated by single and double excitations of electrons from the first-order (reference) configuration to other orbitals. These provide more accurate ASFs when combined, as single excitations can account for deficiencies in the radial wavefunction, and double excitations can account for electron-electron correlations. We do not consider triple excitations in this work since electron-electron-electron correlations are negligable. This is a valid assumption as shown in other work the third-order effects due to triple electron correlations impact the final energy eigenvalues by at most 10^{-6}, or for scandium Kα, 0.004 eV. [8, 20, 21, 29]. With higher-order CSFs being considered, the required computing time increases rapidly - there are four first-order, 1,114 second-order (one excitation), and 144,925 third-order (two excitations) CSFs for the initial (pre-transition) scandium atom, to allow for excitations up to the $6s$ shell for the diagram line calculations. Since the number of CSFs required increased rapidly, and the upper limit of the third-order effects are known to be insignificant, with current technology it is unnecessary to compute the third-order and above terms.

When implementing shake-off events we use the sudden impact approximation [30]. This dictates that the removal of electrons occurs adiabatically, with no time for the system to relax and reach a new state function. This one-step process is a well supported approximation [31–33], especially when the perturbing energy is well above the K-threshold for the given element, which is the case for all empirical studies we will compare our theoretical results with.

How the theory is put in to practice within the GRASP2K framework is detailed, in brief, in the appendix.

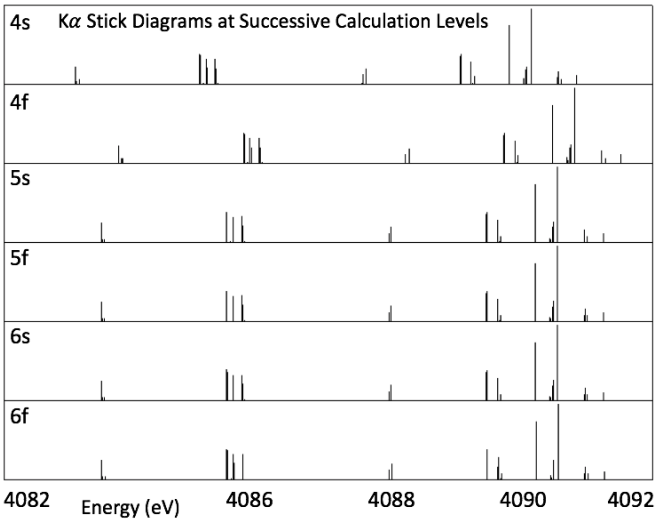

FIG. 1. Eigenvalue spectrum (stick diagrams) for the Sc $K\alpha$ diagram transition, calculated for the $4s$ (first-order), $4f, 5s, 5f, 6s$ and $6f$ (third-order) shells. There is clear convergence as the calculation is expanded to higher levels. The heights of the sticks are a measure of their relative intensity. A representation of convergence of the satellites are presented in Fig. 2

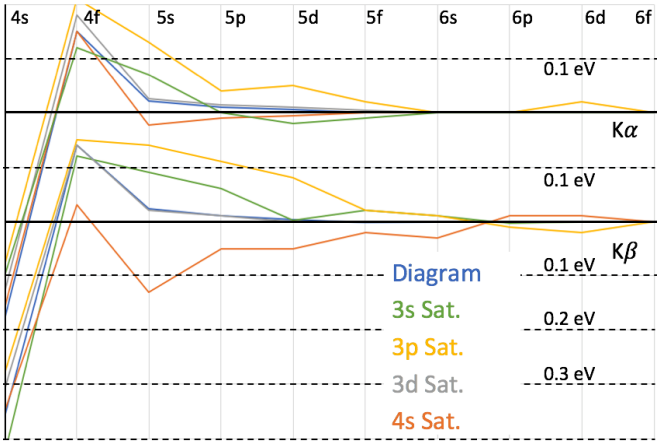

FIG. 2. A measure of convergence for the energy eigenvalues of the different transitions as more shells are used in calculating the ASFs. We take the centre of mass of the energy eigenvalue spectrum (sticks) in each transition calculation, and present the difference between their $6f$ level of calculation and the nl level. Each horizontal grid line represents 0.1 eV. Clearly, the $K\alpha$ calculations converge faster than the $K\beta$. However, both are well-converged by the $6f$ level. These values are given in Table IV for Kα, and Table V for Kβ

SCANDIUM $K\alpha$ AND $K\beta$ TRANSITION ENERGIES

The previous section outlines how the energy eigenvalues are created for each transition. In this section we present the results for the diagram line, $3s, 3p, 3d$, and $4s$ shake-off satellites for both the $K\alpha$ and $K\beta$ transitions. We do not discuss $n = 2$ shake-events herein, since the energy range of the experimental data does not reach the region of these high energy satellites.

For each transition a first-order (no excitations) calculation is done at the $4s$ level which provides a good approximation for the energy eigenvalues (typically within 1%). Then we introduce electron-electron correlations for third-order CSFs with double excitations up to the $6f$ shell. Fig. 1 presents the eigenvalue spectra (stick diagrams) for the $K\alpha$ diagram line at successive shells, convergence of eigenvalues at higher levels is clearly observed. We quantify this convergence for both diagram and all satellite lines by calculating the difference between the energy eigenvalue centre of mass (weighted means) at the $6f$ and nl levels of calculation (Fig. 2). It is clear there is great convergence after the $5s$ level for $K\alpha$ calculations, and after the $6s$ level for $K\beta$.

The results at the $6f$ level for both diagram and all satellite lines computed are shown in Fig. 3 for $K\alpha$ and Fig. 4 for $K\beta$. Several features in Figs. 3 and 4 are important. First, the stick heights are indicative of probabilities relative to each other within the same transition, not between different transitions. The $4s$ shake-off satellite has eigenenergies very similar to the diagram line, due to the very small potential of the $4s$ electrons. These border the conduction band for scandium metal and do not affect the overall atomic potential greatly. The $3s$ and $3p$ satellites in general give energy spectra higher than the diagram line for both $K\alpha$ and $K\beta$ while the $3d$ satel-

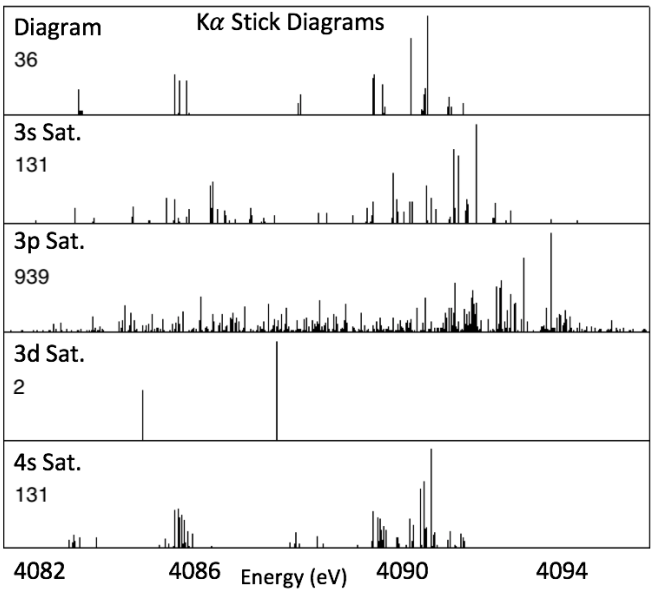

FIG. 3. Energy eigenvalue spectra for each of the transitions for Sc $K\alpha$. The height of each stick is representative of its probability relative to the other sticks in the same transition, but not between transitions. The number of energy eigenvalues is given below the transition label.

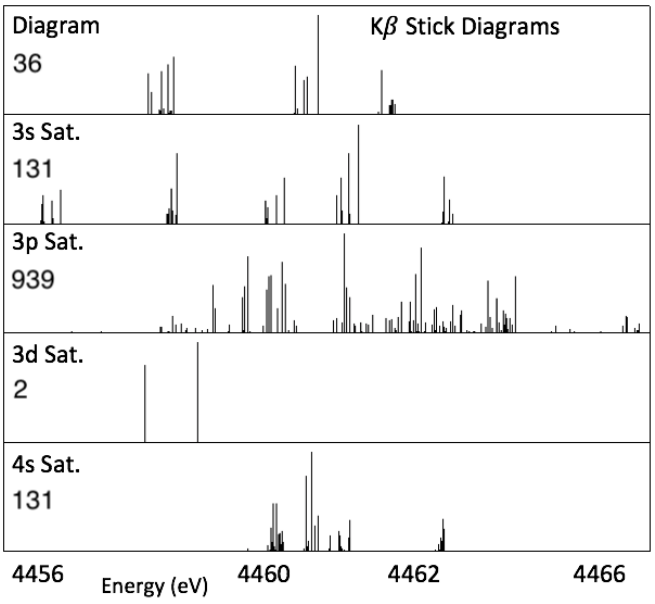

FIG. 4. Energy eigenvalue spectra for each of the transitions for Sc $K\alpha$. The height of each stick is representative of its probability relative to the other sticks in the same transition, but not between transitions. The number of energy eigenvalues is given below the transition label.

lite has a lower energy for $K\alpha$ and $K\beta$. Classically, one might expect that a double ionised atom should always have greater transition energies due to a greater Coulomb potential. However, this reasoning is simplistic and fails to account for electron cloud shielding, quantum coupling effects, and spin coupling effects. Overall, attempting to predict subtle energy changes of relativistic quantum mechanics from intuition is at least a fraught process. Each of these features was noted in Ref. [22]. This previous work raised the possibility of multiple distinct ground states for the scandium atom, the [Ar]$3d^1 4s^2$ as well as [Ar]$3d^0 4s^2$, [Ar]$3d^1 4s^1$, and [Ar]$3d^1 4s^0$. We have investigated this question for Cu [20]. They noted that the different ground states had minimal impact upon the overall profile. Our earlier study found potentially significant effects on the spectral profile. In both studies, the canonical ground state, (in this case [Ar]$3d^1 4s^2$), provided the best fit to experimental spectra, as might be theoretically hoped-for. Of course, strong band or molecular bonding effects could change this, yet such are not observed for the metal species providing the reference experimental data. Herein we will (therefore) only consider the canonical ground state.

The number of energy eigenvalues arises from Fermi's Golden Rule for E1 transitions. For both $K\alpha$ and $K\beta$ there are 36 nondegenerate eigenvalues for the diagram transition, 131 for the $3s$ (and $4s$) satellite, 939 for the $3p$ satellite, and two for the $3d$ satellite. This pattern makes sense, as the removal of a $3s$ or $3p$ electron from the ground state Sc atom increases the number of electron holes, and therefore possible j values, while the removal of the lone $3d$ electron reduces the atom to a closed system with only two possible energy eigenvalues for the $K\alpha_1$ and $K\alpha_2$, or $K\beta_1$ and $K\beta_3$ transitions.

One might expect that the more eigenvalues a transition has, the more difficult the calculation is to perform. In this case, convergence is more readily achieved with the $3p, 4s$ satellites and diagram transitions than the $3d$ satellite. The $3s$ satellite has roughly the same convergence rate as the $3d$. However, computation time does certainly increase with the number of eigenvalues.

Whilst Fig. 2 gives confidence in the convergence of the calculations for each successive expansion there are several other methods to monitor convergence by examining the gauge ratio. The tables representing these are given in Appendix II. There is the ratio of transition amplitude between relativistic length (Babushkin) and velocity (Coulomb) gauges for the same energy level of calculation (A^L/A^v), shown in Tables. VIII and IX. Also, there is the ratio of transition amplitude for succesive energy level calculations for the same gauge, shown in Tables. X and XI. Last, the convergence of the peak energy eigenvalue, rather than the centre of mass of the energy eigenvalues. The two gauge related measurements all tend toward unity as the ASF is expanded to include higher energy levels. This suggests that as the CSF set is enlarged our (total) wavefunctions are converging to represent the true atomic state wavefunction. This is strengthened with the centre of mass energy eigenvalue (Fig. 2, Tables. IV and V) and peak energy eigenvalue (Tables. VI and VII) all converging on a value.

COMPARISON WITH EXPERIMENTAL DATA

The difficulty of an *ab initio* scandium transition calculation partially explains the reason for a lack of scandium theory in the literature. There are also relatively fewer empirical studies than the other $3d$ transition metals. Only four relative energy experiments [22, 32, 34, 35] and two absolute energy experiments [9, 10] have been published since Bearden, Ref. [36], in 1967.

To test the computed energy eigenvalues and their relative intensities we compare our results with experimental data from Dean et al. [9, 10]. Other data sets, namely Ito et al. [32, 35], Kawai et al. [34], and Anagnostopoulos et al. [22] were concerned with the satellite structure of the profile and therefore did not perform an absolute energy calibration; whereas Dean et al. was an absolute energy measurement, as well as being concerned with satellite structures. Furthermore, Dean et al. compares their results to these other works.

The data is fit with a profile, A, which is the sum of n Lorenztian Profiles centred around each energy eigenvalue, where n is the number of nondegenerate energy eigenvalues for the specific transition (the number of

sticks):

$$A(E) = I \sum_{i}^{n} C_i \frac{W}{(E - E_i)^2 + (W)^2} \quad (5)$$

where the *ith* eigenvalue has energy, E_i, and relative amplitude, C_i; each Lorentzian Profile shares a common width, W; and I is a normalising coefficient. The E_i and C_i parameters are calculated in GRASP. The free parameters are W, I, with I being constrained. To determine any systematic energy offset between theory and experiment, we apply a constant energy shift, E', to the whole spectrum. To test the shake-off hypothesis for the asymmetries apparent in the spectra, fits will be performed for a variety of combinations of satellite diagram and satellite spectra. Therefore, our full model has the form:

$$B(E) = \sum_{a}^{m} I_a \sum_{i}^{n} C_{a,i} \frac{W_a}{(E - E_{a,i} - E_a)^2 + (W_a)^2} \quad (6)$$

where B is the spectrum made up of m sets of energy eigenvalues, given from the diagram and satellite lines; each subset is denoted by subscript, a. I_a is a normalising coefficient for each transition and can be treated as a fractional intensity for each transition.

Observing how the goodness of fit changes for different selections of energy eigenvalue enables us to test the necessity of various satellite contributions. The approach to investigate combining satellite eigenvalue spectra to fit the experimental data is subdivided as follows: α, only the diagram; $\alpha 3d$, the diagram and $3d$ satellite; $\alpha 3p$, the diagram and $3p$ satellite; $\alpha 3pd$, the diagram, $3p$ and $3d$ satellites; and $\alpha 3spd$, the diagram, $3s$, $3p$, and $3d$ satellites. The same approach is implemented for fitting the $K\beta$ profiles, replacing the α with a β in the naming of the methods. However, for $K\beta$, we include the $4s$ satellite in two methods and add '$4s$' to the naming convention. The results for the free parameters, widths, W_a, fractional area, I_a, energy shift, E_a and the goodness-of-fit, χ^2_r are given in Tables I and II. Plots of the fits are shown in Figs. 6 to 15.

The parameters I_a are representative of the probability of the specific transition. These are normalised such that the total probability adds to unity. Some work uses notation which sets the diagram intensity at unity and normalises the satellite transition probability to this. However, we believe having $\Sigma I_a = 1$ is optimal. The parameters E_a test how well the final eigenvalues converge to the experimental profile. Higher magnitudes of E_a indicate systematic errors in either the theoretical calculations or in the experimental values for Sc $K\alpha$ and Sc $K\beta$. Since only one high resolution absolute energy experiment has been done on these X-ray lines, it is not possible at this time to make a strong comment on which cause might be dominant.

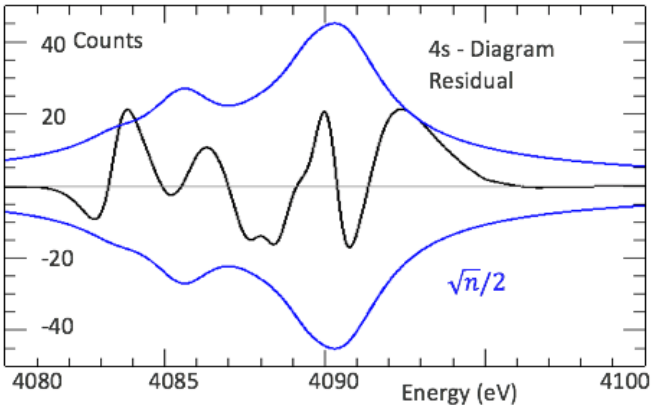

FIG. 5. The difference between the diagram and $4s$ transitions (black) enveloped by half of the $\sqrt{n}$ counting error (blue). The fact that the residual lies within $\sqrt{n}/2$ almost everywhere indicates that attempting to fit the $4s$ satellite line would be impossible since it would be swallowed up by the diagram line. Therefore, the reported intensity of the diagram line is really the intensity of the sum of diagram and $4s$ satellite spectra.

As mentioned, we do not fit the $4s$ satellite for the $K\alpha$ profile. This is valid since the satellite and diagram profiles overlap so significantly that a residual between the two is always within the $\sqrt{n}$ Poissonian counting error, in fact, it is almost entirely within half that (Fig. 5). Therefore, the derived probability for the diagram line is in fact a prediction about the probability of the diagram and the $4s$ satellite combined. Future work should be able to resolving the two. Initially it was not clear whether the same was true for the $K\beta$ $4s$ satellite. However, the inclusion of the $4s$ satellite in the fitting profile makes only minor improvement to the χ^2_r measure of the fit and has an intensity lower than the $3s$ satellite profile which is unrealistic. Therefore, we make the same claim for $K\beta$ as we do with $K\alpha$ which is that the $4s$ satellite cannot be separated from the diagram line at the current level of resolution.

One hypothesis for attempting to explain the asymmetry of the profiles was that the diagram line spectra represent multiple energy eigenvalues and may define the asymmetry. Nonrelativistic quantum theory suggests a $1s^{-1} \rightarrow 2p^{-1}$ transition would have one energy eigenvalue seen as a symmetric Lorentzian profile. Considering electron spin would give separate $K\alpha_1$ and $K\alpha_2$ transitions from $2p^{-1}_{3/2}$ and $2p^{-1}_{1/2}$ final states respectively. However, fully relativistic quantum theory leads to non-degenerate transitions between all initial and final momenta for the relevant electron configurations, described by Fermi's Golden Rule. We only consider electric dipole (E1) transitions as the next most significant transitions are suppressed by order $(\frac{Z}{137})^2$ - electric quadrupole (E2) and magnetic dipole (M1).

For the diagram transition $1s^{-1} \rightarrow 2p^{-1}$ there are thirty-six eigenvalues (Fig. 3). This is already an asym-

Method:		χ^2_r	α_1	α_2	$3s^{-1}$	$3p^{-1}$	$3d^{-1}$
α	W_a (eV)	14.9	1.86	1.54	-	-	-
	I_a		0.65	0.35*	-	-	-
	E_a (eV)		+0.54	+0.54*	-	-	-
$\alpha 3p$	W_a (eV)	3.28	1.83	1.63	-	2.21	-
	I_a		0.48	0.23*	-	0.29	-
	E_a (eV)		+0.46	+0.46*	-	+0.63	-
$\alpha 3d$	W_a (eV)	10.7	1.89	2.05	-	-	1.10
	I_a		0.57	0.29*	-	-	0.14
	E_a (eV)		+0.55	+0.55*	-	-	+0.02
$\alpha 3pd$	W_a (eV)	1.88	1.65	1.55	-	2.04	1.55
	I_a		0.49	0.27*	-	0.14	0.10
	E_a (eV)		+0.34	+0.34*	-	+0.18	+0.07
$\alpha 3spd$	W_a (eV)	1.60	1.65	1.57	2.42	2.28	1.98
	I_a		0.49	0.26*	0.02	0.13	0.10
	E_a (eV)		+0.34	+0.34*	+0.38	+0.18	+0.07

TABLE I. Results for the parameters W_a Lorentzian full-width-half-maximum, I_a, fractional intensity, and E_a, energy shift from fitting various combinations of calculated Sc $K\alpha$ diagram and satellite transitions. Values given are for the goodness-of-fit, χ^2_r, widths (FWHM), W_a, fractional area, I_a, and energy shift, E_a. A positive energy shift defines a shift of energy eigenvalues towards higher energy. The plots of each method of fitting are given in Figs. 6 to 14.
* These values are not free, rather, are given for completeness but come from fitting the diagram line as a single profile with individual $K\alpha_{1,2}$ widths.

Method:		χ^2_r	$\beta_{1,3}$	$3s^{-1}$	$3p^{-1}$	$3d^{-1}$	$4s^{-1}$
β	W_a (eV)	8.24	2.93	-	-	-	-
	I_a		1	-	-	-	-
	E_a (eV)		+0.41	-	-	-	-
$\beta 3p$	W_a (eV)	7.03	2.46	-	1.75	-	-
	I_a		0.68	-	0.32	-	-
	E_a (eV)		+0.32	-	+0.63	-	-
$\beta 3d$	W_a (eV)	4.24	2.57	-	-	3.71	-
	I_a		0.74	-	-	0.26	-
	E_a (eV)		+0.41	-	-	+0.12	-
$\beta 3pd$	W_a (eV)	1.87	1.67	-	2.44	3.25	-
	I_a		0.65	-	0.21	0.14	-
	E_a (eV)		+0.35	-	+0.51	+0.40	-
$\beta 3spd$	W_a (eV)	1.45	1.48	3.06	2.37	2.48	-
	I_a		0.66	0.04	0.17	0.13	-
	E_a (eV)		+0.32	+0.35	+0.46	+0.37	-
$\beta 3spd4s$	W_a (eV)	1.42	1.44	3.09	2.38	2.43	3.63
	I_a		0.65	0.03	0.13	0.18	0.02
	E_a (eV)		+0.36	+0.34	+0.25	+0.38	+0.53

TABLE II. Results for the parameters W_a Lorentzian full-width-half-maximum, I_a, fractional intensity, and E_a, energy shift from fitting various combinations of calculated Sc $K\beta$ diagram and satellite transitions. Values given are for the goodness-of-fit, χ^2_r, widths (FWHM), W_a, fractional area, I_a, and energy shift, E_a. A positive energy shift defines a shift of energy eigenvalues towards higher energy. The plots of each method of fitting are given in Figs. 7 to 15.

metric profile and can represent the hypothesis that no satellite lines are needed ,and the asymmetry in X-ray spectra is described by the diagram profiles alone. However, this hypothesis is outdated and it is not sufficient to describe the asymmetry in the experimental data, as seen in Figs. 6 and 7 and the poor χ^2_r values. Therefore, we perform shake-off calculations to determine whether these are necessary to describe the asymmetries, and whether they are sufficient, or if there is still room for the remaining hypotheses.

From the improving χ^2_r, the $3s$, $3p$, and $3d$ satellites appear essential for characterising the $K\alpha$ profile of scandium. This is consistent with previous work done on other $3d$ transition metals.

The issue of separating the $4s$ satellite and the diagram profiles is noted for Sc in [22] and other $3d$ transition metals in [20]. This issue is related to the ambiguous ground state of atomic $3d$-group elements. Anagnostopoulos et al. have either $[\mathrm{Ar}]3d^14s^2$ or $[\mathrm{Ar}]3d^14s^1$ as the ground states, the former being our ground state and the latter being what we consider a $4s$ shake-off. The claim being made by both Anagnostopoulos et al. and this work is that the electron in the $4s$ shell is largely in the conduction band of the metal lattice and has very little impact on both Kα and Kβ energy profiles. We prove this claim

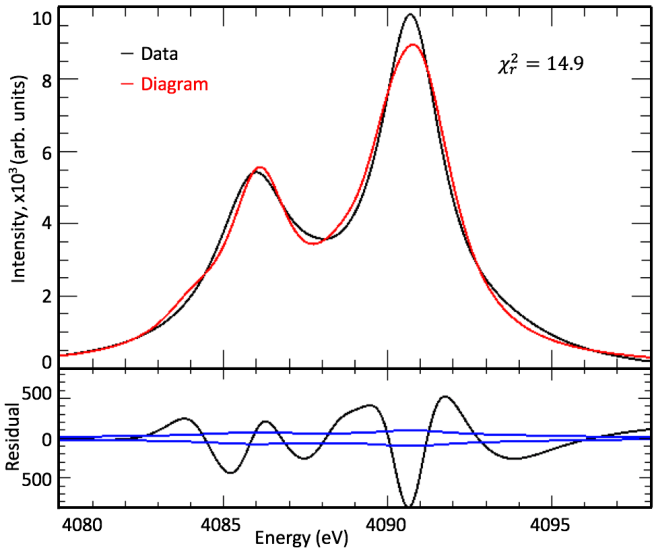

FIG. 6. Fit of the $K\alpha$ diagram profile to the data. Clearly, the fit is poor requiring additional asymmetry from e.g. additional satellite contributions.

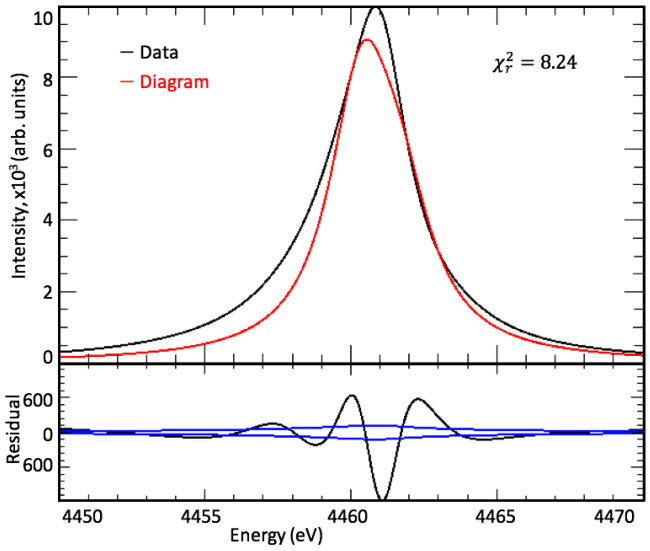

FIG. 7. Fit of the $K\beta$ profile with only the calculated diagram line spectrum. The values for widths, W_a, fractional area, I_a, and energy shift, E_a are in Table II. The goodness of fit, χ_r^2, is 8.24 which is not a good fit. Suggesting that the satellite lines are needed to properly characterise the spectrum.

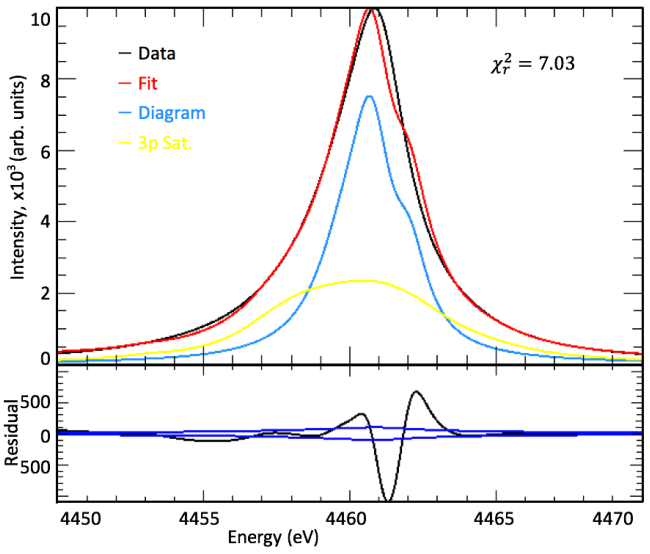

FIG. 9. Fit of the $K\beta$ profile with the calculated diagram line and $3p$ satellite spectra. The values for widths, W_a, fractional area, I_a, and energy shift, E_a are in Table II. The goodness of fit, χ_r^2, 7.03, is only a slight improvement on the diagram-only fit.

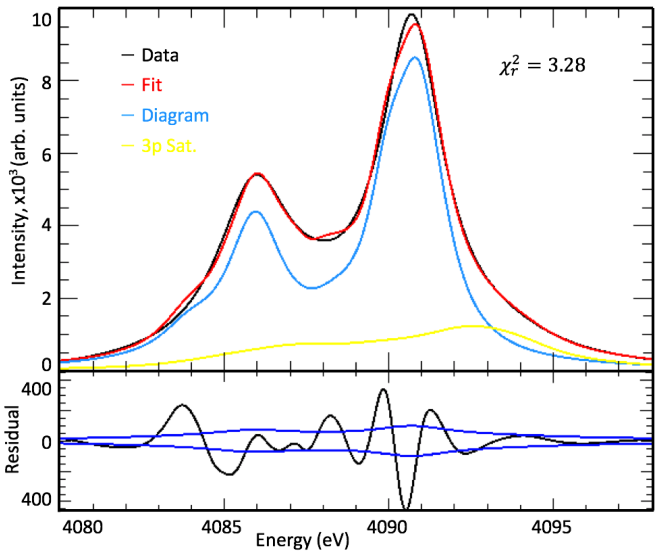

FIG. 8. Fit of the $K\alpha$ diagram and $3p$ satellite spectra to the data. The values for widths, W_a, fractional area, I_a, and energy shift, E_a are in Table I. The goodness of fit, χ_r^2, 3.28, is an impressive improvement to Fig. 6 suggesting that the $3p$ satellite exists and supporting the hypothesis that additional satellites are required to explain the observed experimental spectrum.

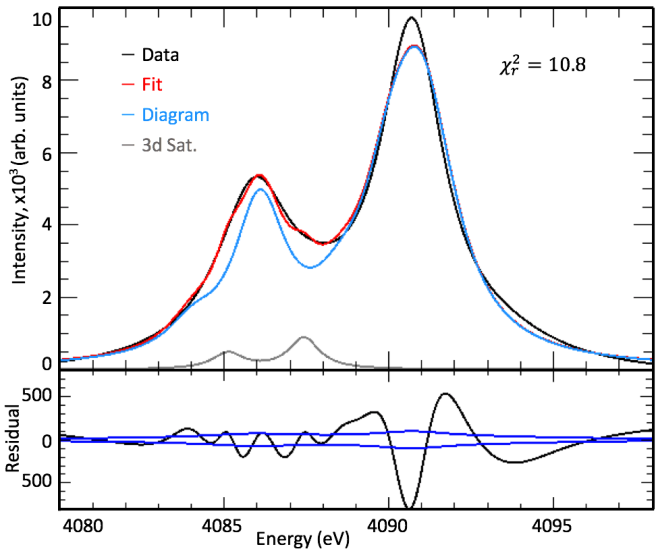

FIG. 10. Fit of the $K\alpha$ diagram and $3d$ satellite spectra to the data. The values for widths, W_a, fractional area, I_a, and energy shift, E_a are in Table I. The goodness of fit, χ_r^2, 10.7, is an improvement on fitting with the diagram alone.

for Sc Kα by fitting the profile of a $4s$ satellite to the diagram line and showing that, given our fitting parameters, the two profiles overlap within error. Future work which obtain *ab initio* calculations of profile width and amplitudes will test this hypothesis by reducing the free parameters in the fitting. However, without higher resolution scans of Sc K-series radiation has been taken this question may not be answered definitively.

For the meantime we report on the $n = 3$ satellites and how their existence is essential for answering the asymmetry question in characteristic radiation.

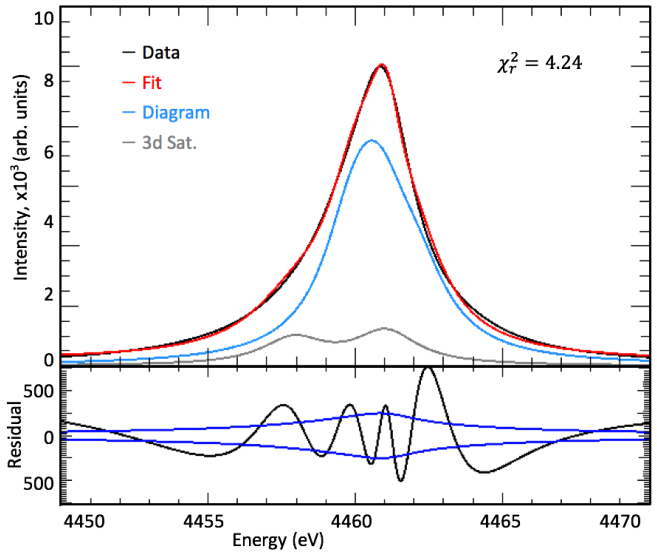

FIG. 11. Fit of the $K\beta$ profile with the calculated diagram line and $3d$ satellite spectra. The values for widths, W_a, fractional area, I_a, and energy shift, E_a are in Table II. The goodness of fit, χ_r^2, 4.24, is a significant improvement upon the diagram only case.

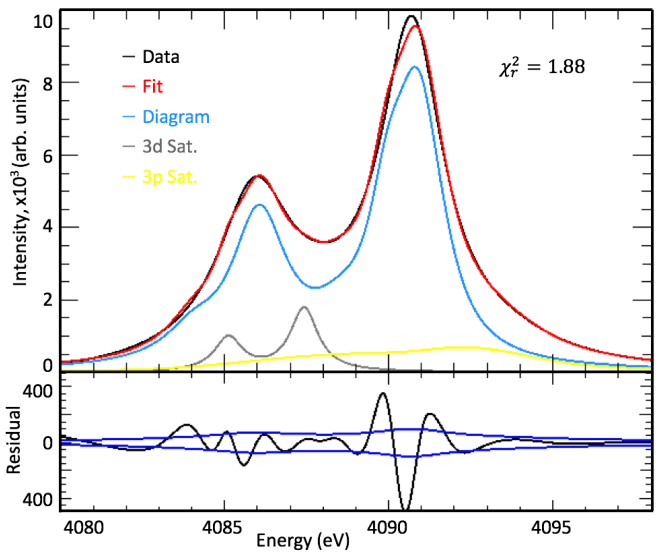

FIG. 12. Fit of the $K\alpha$ diagram, $3p$, and $3d$ satellite spectra to the data. The values for widths, W_a, fractional area, I_a, and energy shift, E_a are in Table I. The goodness of fit, χ_r^2, 1.88, is better than the diagram with either the $3p$ or $3d$ alone suggesting that both satellite lines exist and supports our hypothesis.

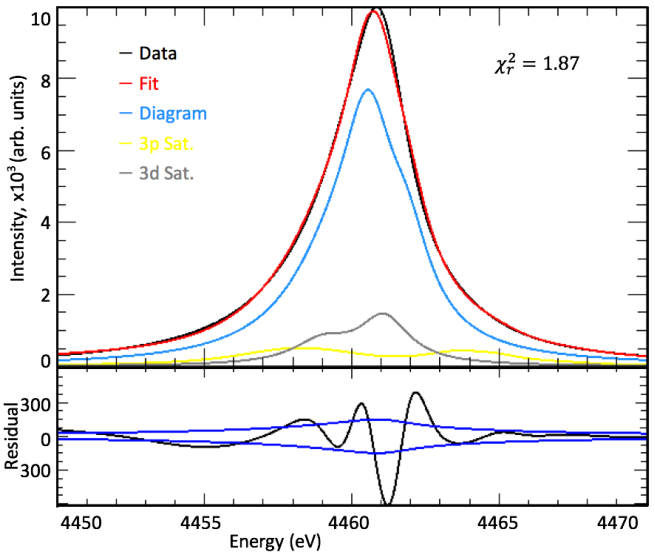

FIG. 13. Fit of the $K\beta$ profile with the calculated diagram line, $3p$, and $3d$ satellite spectra. The values for widths, W_a, fractional area, I_a, and energy shift, E_a are in Table II. The goodness of fit, χ_r^2, 1.87, suggests that both satellite lines are important.

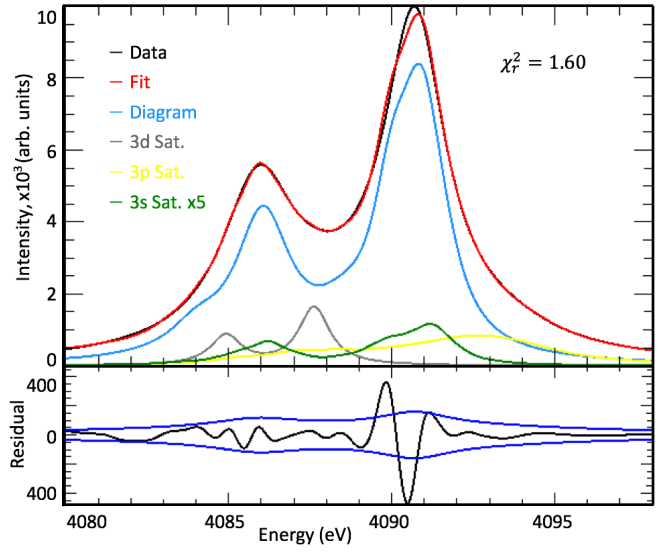

FIG. 14. Fit of the $K\alpha$ diagram, $3s$, $3p$, and $3d$ satellite spectra to the data. The values for widths, W_a, fractional area, I_a, and energy shift, E_a are in Table I. The goodness of fit, χ_r^2, is 1.60 which is the best fit suggesting that all satellite lines are important to the fit. Being the best fit for Kα, this is the fit that we suggest readers to use for any future work.

MEASURE OF CENTRAL ENERGY

In the previous section, we allowed the energies of the transitions to shift slightly to best fit the satellite structure of the experimental profile. The energy shift allowed the semi-empirical fits of amplitude and width to be found. Without this energy shift, the asymmetries would not have been well accounted for by satellite transitions and amplitudes and widths would be incorrect.

This highlights the dual purpose of this work. We are testing the ability for relativistic quantum mechanic equations and complex atomic physics to both account for the asymmetry in radiative X-ray lines and measure

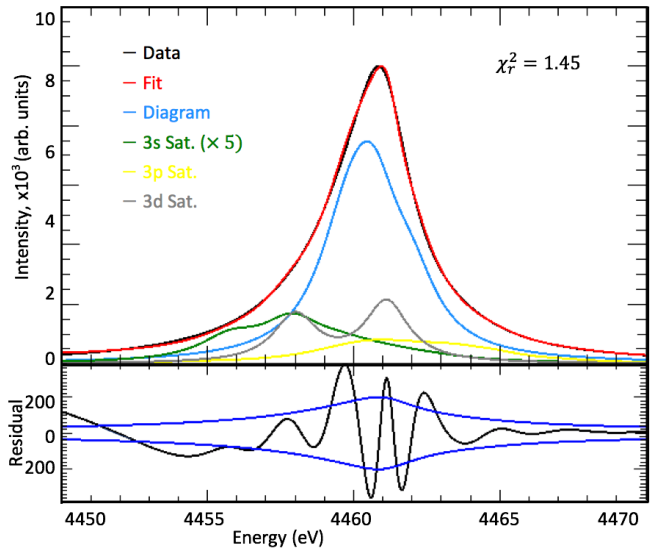

FIG. 15. Fit of the $K\beta$ profile with the calculated diagram line, $3s$, $3p$, and $3d$ satellite spectra. The $3s$ satellite has been enlarged by a factor of five to make easier to observe. The values for widths, W_a, fractional area, I_a, and energy shift, E_a are in Table II. The goodness of fit, χ_r^2 is 1.45. Being the best fit for Kβ, this is the fit that we suggest readers to use for any future work.

the centre of energy of the entire spectrum.

The energy shift is due to systematic errors between the GRASP energy eigenvalue output and the characterised energy spectrum obtained through experiment.

The previous theoretical calculation for Sc $K\alpha$ and $K\beta$ used an earlier development of GRASP and also allowed an energy shift, however, their shifts were of order 1 eV - 2 eV [22]. While impressive for its time with limited computing power of the late 1990s it has been superseded. In this work the best fitting methods required only shifts of the diagram line of 0.330 eV for $K\alpha$ and 0.363 eV for $K\beta$, approximately four times less than the previous work.

Allowing an energy shift is important to test the necessity of shake-events for characterising the asymmetries in X-ray transition lines. However, arriving at an *ab initio* calculation of an energy we must, of course, use the *ab initio* calculated energy eigenvalues.

There are several measures of energy that are useful across the many applications of characteristic X-ray radiation. These are the peak energy, the energy of the peak of the experimental profile; the reconstructed characterisation peak energy, E($K\alpha_1^0$), E($K\alpha_2^0$), E($K\beta^0$), which are defined as the peak of the characterisation with zero Gaussian width; and the centre of mass energy. When fitting atomic structure calculations to experimental spectra we can compare the reconstructed peak energies of the profile to experimental reconstructed peak energies to obtain an approximation of accuracy. For theoretical work, the peak energy and reconstructed peak energy are identical since Gaussian width is zero because we are fitting to experimental data with the Gaussian width removed. It is important to keep this in mind when comparing theoretically derived energies to experimental values. Especially those which have high Gaussian width and for older experiments since these distinctions are only made in more recent publications.

Fortunately, Refs [9, 10] provide values for all three measures of central energy. However, Bearden does not and since Bearden's work is from the 1960s it is likely there is a high level of Gaussian width. This is not reported and we are unable to recharacterise his value for better comparison. Furthermore, the previous theoretical calculation mentioned (Anagnostoupolos et al. [22]) does not report their energy eigenvalues on a fixed energy axis since their purpose was to characterise the asymmetry of the profiles, and not calculate an *ab initio* central energy. The work by Deslattes et al. [8] includes a scandium $K\alpha$ and $K\beta$ theoretical energy calculation from an unpublished source. This is not ideal, however, it is the only other like-for-like comparison that we can make from the literature.

We reconstruct our profile from method $(\alpha/\beta)3spd$ from Tables I and II setting the value $E_a = 0$. The peak of this profile is taken and reported in Table III along with the *ab initio* theoretical results from Deslattes et al. [8], and the only two absolute energy experiments in the literature of Dean et al. [9, 10] and Bearden [37]. While other experiments on scandium $K\alpha$ and $K\beta$ have been done they have all been relative energy measurements using the result from Bearden to calibrate for their energy. These are experiments with the purpose of characterising the asymmetry of the scandium characteristic x-ray profile rather than calculating its absolute energy and therefore not suitable for comparisons here. These are works of Ito et al. [32, 35], Kawai et al. [34] and the aforementioned Anagnostopoulos et al. [22].

The uncertainty comes from the mean square summation of individual sources of uncertainties from the fitting procedure of width, amplitude, and relative intensity of the satellite transitions. We see that the difference between the previous theoretical result to experiment, and our calculation to the same experiment, has reduced from 0.549 eV to 0.330 eV for Kα_1^0 and 0.498 eV to 0.342 eV for Kα_2^0. A remarkable reduction from 1.745 eV to 0.363 eV has been achieved for the Kβ^0 centroid. These new results are impressive, but still lie 4σ away from the experimental results, when using the summation of errors from theory and experiment. Therefore, further experimental work is welcomed. However, these results clearly bring the understanding of Sc towards that of other $3d$ transition metals, which have long been considered the benchmark for characteristic X-ray energies and calibration, such as Cu.

Source	Transition	Energy	Uncertainty	Difference
This Work	$K\alpha_1^0$	4090.369	0.069	-
	$K\alpha_2^0$	4085.584	0.074	-
	$K\beta^0$	4460.482	0.13	-
Bearden [36]	$K\alpha_1^0$	4090.74	0.19	+0.371
	$K\alpha_2^0$	4085.95	0.85	+0.364
	$K\beta^0$	4460.44	0.47	-0.045
Dean et al. [9]	$K\alpha_1^0$	4090.699	0.010	+0.330
	$K\alpha_2^0$	4085.926	0.018	+0.342
Dean et al. [10]	$K\beta^0$	4460.845	0.0092	+0.363
Deslattes et al. [8]	$K\alpha_1^0$	4090.15	0.44	-0.219
	$K\alpha_2^0$	4085.43	0.42	-0.156
	$K\beta^0$ *	4462.59	0.80	+2.105

TABLE III. Results for energy centroid from this work, and previous experimental (Dean et al. and Bearden) and theoretical (Deslattes et al.) work. All values are in eV.
* Deslattes et al. give $K\beta_1^0$ and $K\beta_3^0$ component energies and not a reconstructed peak energy of the full spectrum. Therefore, to compare to our value we reconstruct the peak energy using their values and experimental values for width and amplitude of the profiles. Details of this reconstruction are found in Dean et al. [10].

CONCLUSION

The Sc $K\alpha$ and $K\beta$ x-ray lines have been calculated using an *ab initio* approach. These results show that asymmetries in X-ray spectra are the result of satellite lines arising from multi-vacancy shake-off events. These are clearly the dominant mechanism for asymmetries, and therefore there is little room left for other phenomena in comparisons of Sc metal with atomic theory. Further to obtaining an *ab initio* calculation representing spectral asymmetries, we have shown that *ab initio* calculations can achieve better than 0.5 eV accuracy for the centre of mass energy for the Sc Kα and Kβ profiles. The ability to obtain centres of mass energy with *ab initio* calculations is of great interest to the wider community, including industry, especially those in X-ray fluorescence fields, as well as the scientific community for use on calibrations of crystallographic experiments amongst other.

We reduce the previous error for the centre of energy calculation of 55σ to one of 33σ using the experimental uncertainty alone. This seemingly large error is indicative of the incredibly precise experimental value and represents a leap in the right direction for *ab initio* MCDHF calculations. There are important avenues for further research for both theory and experiment, since the results continue to show a 4σ divergence when the error of theory and experiment are summed together. Since there is only one absolute energy measurement in the literature to compare with within the last fifty years (since Bearden [36]), there is potential for future work to characterising the Sc Kα and Sc Kβ profiles.

Convergence of both energy eigenvalues and gauge ratios, as the active set of CSFs is expanded to include wavefunctions of higher energy levels, represents the consistency of these results within the MCDHF framework. The methods implemented here naturally extend to other systems and leaves little room for uncertainty in the implementation of the MCDHF method used.

Whilst ab initio calculations for energies are performed the widths of each transition and relative amplitudes of shake events are fitted as free parameters and therefore semi-empirical. This is an area for future work along with fitting Auger Emission profiles. There are difficulties with ab initio shake probabilities and calculating widths from first principals that are beyond the scope of this paper, Proving energy eigenvalues can be calculated for complex open shell atomic systems using the best standards for relativistic quantum mechanics is essential in its own right.

Ultimately, this provides a much needed advance for theoretical relativistic quantum mechanics. The $3d$ transition elements are a bedrock for state-of-the-art atomic physics and the marriage of results from both empirical and theoretical works, for both centre of energies and asymmetries is essential to provide a consistent framework for the most complex optical and atomic physics questions in to the future.

BIBLIOGRAPHY

* jonathan.dean@unimelb.edu.au
† corresponding: chantler@unimelb.edu.au

[1] M. Hansson, G. Berg, and M. Isaksson, X-Ray Spectrometry **37**, 37 (2008).
[2] Šmíd, M. And Renner, O. And Colaitis, A. And Tikhonchuk, V. T. And Schlegel, T. And Rosmej, F. B., Nature Communications **10**, 4212 (2019).
[3] V. Jonauskas and G. Gaigalas and S. Kučas, Atomic Data and Nuclear Data Tables **98**, 19 (2012).
[4] Duro, Refiz, Dauser, Thomas, Grinberg, Victoria, Miskovicová, Ivica, Rodriguez, Jérôme, Tomsick, John, Hanke, Manfred, Pottschmidt, Katja, Nowak, Michael A., Kreykenbohm, Sonja, Bel, Marion Cadolle, Bodaghee, Arash, Lohfink, Anne, Reynolds, Christopher S., Kendziorra, Eckhard, Kirsch, Marcus G. F., Staubert, Rüdiger, and Wilms, Jörn, Astronomy and Astrophysics **589**, A14 (2016).
[5] F. M. Fornasini, J. A. Tomsick, M. Bachetti, R. A. Krivonos, F. Fürst, L. Natalucci, K. Pottschmidt, and J. Wilms, The Astrophysical Journal **841**, 35 (2017).
[6] K. A. Weaver, J. Gelbord, and T. Yaqoob, The Astrophysical Journal **550**, 261 (2001).
[7] C. S. Reynolds and A. C. Fabian, The Astrophysical Journal **675**, 1048 (2008).
[8] R. D. Deslattes, E. G. Kessler, P. Indelicato, L. de Billy, E. Lindroth, and J. Anton, Reviews of Modern Physics **75**, 35 (2003).
[9] J. W. Dean, C. T. Chantler, H. A. Melia, and L. F. Smale, Journal of Physics B **52**, 165002 (2019).
[10] J. W. Dean, C. T. Chantler, L. F. Smale, and H. A. Melia, Journal of Physics B **53**, 205004 (2020).
[11] M. Siegbahn and W. Stenstrom, Phys. Zeits. **17**, 318 (1916).
[12] S. I. Salem, G. M. Hockney, and P. L. Lee, Physical Review A **13**, 330 (1976).
[13] K. S. Srivastava, R. L. Shrivastava, O. K. Harsh, and V. Kumar, Physical Review B **19**, 4336 (1979).
[14] S. Doniach and M. Sunjic, Journal of Physics C **3**, 285 (1970).
[15] F. K. Richtmyer and L. S. Taylor, Physical Review **36**, 1044 (1930).
[16] L. Parrot, Reviews of Modern Physics **31**, 616 (1959).
[17] M. Deutsch and M. Hart, Physical Review B **26**, 5558 (1982).
[18] G. Wentzel, Annalen der Physik **66**, 437 (1921).
[19] F. Bloch, Physical Review **48**, 187 (1935).
[20] C. T. Chantler, J. A. Lowe, and I. P. Grant, Phys. Rev. A **82**, 52505 (2010).
[21] T. L. Pham, T. V. Nguyen, J. A. Lowe, I. P. Grant, and C. T. Chantler, Journal of Physics B: Atomic, Molecular and Optical Physics **49**, 035601 (2016).
[22] D. Anagnostopoulos, R. Sharon, D. Gotta, and M. Deutsch, Physical Review. A **60**, 2018 (1999).
[23] J. A. Lowe, C. T. Chantler, and I. P. Grant, Radiation Physics and Chemistry **85**, 118 (2013).
[24] C. T. Chantler, T. V. Nguyen, J. A. Lowe, and I. P. Grant, Physical Review A **90**, 1 (2014).
[25] T. V. B. Nguyen, J. A. Lowe, T. L. H. Pham, I. P. Grant, and C. T. Chantler, (2015), The modified GRASP2K package, dubbed version 1.15, is available from `https://www.ph.unimelb.edu.au/~chantler/opticshome/softwarepackagedownloads.html#GRASP2KRCISE`.
[26] K. G. Dyall, I. P. Grant, C. T. Johnson, F. A. Parpia, and E. P. Plummer, Computer Physics Communications **55**, 425 (1989).
[27] F. A. Parpia, C. Froese Fischer, and I. P. Grant, Computer Physics Communications **175**, 745 (2006).
[28] P. Jönsson, X. He, C. Froese Fischer, and I. P. Grant, Computer Physics Communications **177**, 597 (2007).
[29] J. Hoszowska, A. K. Kheifets, J. C. Dousse, M. Berset, I. Bray, W. Cao, K. Fennane, Y. Kayser, M. Kavčič, J. Szlachetko, and M. Szlachetko, Physical Review Letters **102**, 073006 (2009).
[30] T. D. Thomas, Physical Review Letters **52**, 417 (1984).
[31] T. A. Carlson and M. O. Krause, Physical Review **140** (1965), 10.1103/PhysRev.140.A1057.
[32] Y. Ito, T. Tochio, M. Yamashita, S. Fukushima, A. M. Vlaicu, Syrocki, K. Słabkowska, E. Weder, M. Polasik, K. Sawicka, P. Indelicato, J. P. Marques, J. M. Sampaio, M. Guerra, J. P. Santos, and F. Parente, Physical Review A **97**, 52505 (2018).
[33] O. Mauron, J.-C. Dousse, J. Hoszowska, J. P. Marques, F. Parente, and M. Polasik, Phys. Rev. A **62**, 062508 (2000).
[34] J. Kawai, E. Nakamura, Y. Nihei, K. Fujisawa, and Y. Gohshi, Spectrochimica Acta Part B: Atomic Spectroscopy **45**, 463 (1990).
[35] Y. Ito, T. Tochio, H. Ohashi, M. Yamashita, S. Fukushima, M. Polasik, K. Slabkowska, L. Syrocki, J. Rzadkiewicz, P. Indelicato, J. P. Marques, M. C. Martins, J. P. Santos, and F. Parente, Phys. Rev. A **94**, 42506 (2016).
[36] J. A. Bearden, Reviews of Modern Physics **39**, 78 (1967).
[37] J. A. Bearden and A. F. Burr, Reviews of Modern Physics **39**, 125 (1967).
[38] M. Deutsch, G. Hölzer, J. Härtwig, J. Wolf, M. Fritsch, and E. Förster, Physical Review A **51**, 283 (1995).
[39] C. T. Chantler, A. C. Hayward, and I. P. Grant, Physical Review Letters **103**, 2 (2009).
[40] L. Sturesson, P. Jönsson, and C. Froese Fischer, Computer Physics Communications **177**, 539 (2007).

APPENDIX I: GRASP2K IMPLEMENTATION

The level of detail for the presented Sc $K\alpha, \beta$ transition energies is possible due to advances in computation power. The 1995 state-of-the-art calculation on the Cu $K\alpha$ spectrum [38] used only one CSF for the initial and final electron configurations. Furthermore, the $4s$ electron was discounted entirely and no excitations were allowed (only first-order CSFs) [38]. Discounting the $4s$ electron enabled [38] to consider the atom as a closed shell system, greatly reducing convergence time. In 2009, Chantler et al. performed included the $4s$ electron and allowed one and two electron excitations (second-order and third-order CSFs) up to the $5s$ shell [39]. This required just over 20,000 CSFs. We are now able to present calculations that have required simultaneous convergence of over 10^6 CSFs.

We performed this calculation within the GRASP2K framework. The N-electron basis set of CSFs, T are given in the *JJGEN* subroutine [40]. Angular momentum coefficients, $t_T(\alpha\beta)$ and $v_T^K(\alpha\beta\gamma\delta)$ are obtained from *JSPLIT* and *MCDF*. These are used in the Dirac-Coulomb Hamiltonian, rewritten from Eqn. 2 as:

$$H_T = \sum_{\alpha\beta} t_T(\alpha\beta) I_T(\alpha\beta) + \sum_{K;\alpha\beta\gamma\delta} v_T^K(\alpha\beta\gamma\delta) R_C^K(\alpha\beta\gamma\delta) \tag{7}$$

where $I(\alpha\beta)$ is the radial part of the one-electron Hamiltonian, $R_C^K(\alpha\beta\gamma\delta)$ is a radial Slater integral, and greek letters stand for active subshells.

Following this, the radial wavefunction is calculated with numerical integration using the Thomas-Fermi method (*ERWF*). The penultimate step in creating the electron configurations is calculating the angular wavefunctions (*RSCF*). The last step for computing the ASF is by making further QED corrections in *RCI*.

Once the initial and final ASFs are calculated, biorthogonalisation of these two sets of ASFs creates expectation values for the energy eigenvalues. This is done in the *BIOTRA* and *BIOSCL* subroutines. The output of this last step is the stick diagram of eigenvalues for the particular transition.

To increase the chance of successful convergence the above steps are repeated iteratively. Initially, the $1s$ shell ASF is calculated, then using this as an initial guess for the potential when calculating the radial wavefunctions of the $2s$ shell (*ERWF*). Then this potential is used for the $2p$ shell and so on. We follow the Aufbau principle in the ordering of shell energies. Furthermore, allowing for the excitations for third-order CSFs is also done iteratively, using the first-order CSF at the $4s$ shell as the initial guess for the potential of the third-order CSFs at the $4p$ level, then continuing up to the $6f$ level. An example for the Sc $K\alpha$ diagram line energy eigenvalues converging as more shells are included in the calculation of the ASFs is shown in Fig. 1. How the energy eigenvalues converge for all transitions considered in this work are shown in Fig. 2.

Each atomic system is different and has its own challenges. Two major issues in any finite basis computation within an infinite vector space are not obtaining convergence or converging to an incorrect answer. The former issue can be approached with increasing computing capacity and decreasing the distance between nodes. The latter is a problem where the solution obtained is a solution for a local minima in potential, rather than the global minimum. This can be resolved by altering initial conditions or manually removing non-physical wavefunctions.

The $3d$ satellite presented the most serious convergence dilemmas, despite the advanced computations and methodologies. This is surprising, since this satellite has only two eigenvalues and an entirely open $3d$ shell. However, this computation results in many local minima and many convergent answers for wavefunctions which are not physical, with energy eigenvalues that are sometimes tens of eV removed from their true position. Whilst having the issues of incorrect convergence, the $3d$ satellite calculations took very little computing power, especially since the computing power required scales with number of CSFs and number of energy eigenvalues.

Level	4s	4f	5s	5p	5d	5f	6s	6p	6d	6f
Diagram	-0.38	0.15	0.02	0.01	0.01	0	0	0	0	0
3s Sat.	-0.30	0.12	0.07	0.00	0.01	-0.02	-0.01	0	0	0
3p Sat.	-0.28	0.21	0.02	0.01	0.01	0	0	0	0	0
3d Sat.	-0.33	0.18	0.03	0.02	0.01	0.01	0	0	0	0
4s Sat.	-0.36	0.15	-0.02	-0.01	-0.01	0	0	0	0	0

TABLE IV. A table of the convergence values for $K\alpha$ shown in Fig. 2. The convergence of the energy eigenvalues are given as the difference of the centre of mass (weighted mean) of the eigenvalues at a given level to the final (6f) level. '0.00' is for rounding to zero where '0' is an exact zero.

Level	4s	4f	5s	5p	5d	5f	6s	6p	6d	6f
Diagram	-0.36	0.14	0.03	0.01	0.00	0.00	0	0	0	0
3s Sat.	-0.43	0.12	0.09	0.06	0.00	0.02	0.01	0.00	0	0
3p Sat.	-0.28	0.15	0.14	0.11	0.08	0.02	0.00	0.00	0.00	0
3d Sat.	-0.31	0.14	0.02	0.01	0	0	0	0	0	0
4s Sat.	-0.35	0.03	-0.13	-0.05	-0.02	-0.03	0.01	0.00	0	0

TABLE V. A table of the convergence values for $K\beta$ shown in Fig. 2. The convergence of the energy eigenvalues are given as the difference of the centre of mass (weighted mean) of the eigenvalues at a given level to the final (6f) level.'0.00' is for rounding to zero where '0' is an exact zero.

APPENDIX II: OTHER QUANTITATIVE ANALYSES OF CONVERGENCE

Presented here are the many quantitative methods to determine the quality of convergence for these calculations.

Level	4s	4f	5s	5p	5d	5f	6s	6p	6d	6f
Diagram	-0.36	0.11	0.02	0.02	0.02	0	0	0	0	0
3s Sat.	-0.28	0.12	0.06	0.00	0.01	-0.02	-0.01	0	0	0
3p Sat.	-0.23	0.20	0.02	0.01	0.00	0	0	0	0	0
3d Sat.	-0.36	0.17	0.03	0.02	0.01	0.01	0	0	0	0
4s Sat.	-0.33	0.11	-0.01	-0.01	0.00	0	0	0	0	0

TABLE VI. A table of the convergence values for most intense energy eigenvalue for the $K\alpha$ calculations. This would be the 'tallest' stick in the stick diagram Fig. 3. As before, '0.00' is for rounding to zero where '0' is an exact zero. We can see the values are similar to the reciprocal table for the centre of mass energy convergence, Table IV.

Level	4s	4f	5s	5p	5d	5f	6s	6p	6d	6f
Diagram	-0.33	0.14	0.03	0.01	0.00	0.00	0	0	0	0
$3s$ Sat.	-0.45	0.12	0.09	0.06	0.02	0.02	0.00	0.	0	0
$3p$ Sat.	-0.32	0.15	0.05	0.09	0.04	0.02	0.00	0	0	0
$3d$ Sat.	-0.31	0.14	0.02	0.01	0	0	0	0	0	0
$4s$ Sat.	-0.32	0.03	-0.11	-0.05	-0.01	-0.01	0.01	0.00	0	0

TABLE VII. A table of the convergence values for most intense energy eigenvalue for the $K\beta$ calculations. This would be the 'tallest' stick in the stick diagram Fig. 4. As before, '0.00' is for rounding to zero where '0' is an exact zero. We can see the values are similar to the reciprocal table for the centre of mass energy convergence, Table V.

$K\alpha$	$4s$	$4f$	$5s$	$5f$	$6s$	$6f$
Diagram	1.022	1.025	1.013	1.009	1.004	1.003
$3s$ Sat.	1.023	1.022	1.021	1.013	1.010	1.009
$3p$ Sat.	1.019	1.020	1.016	1.016	1.015	1.008
$3d$ Sat.	1.010	1.011	1.007	1.007	1.005	1.005
$4s$ Sat.	1.018	1.019	1.012	1.009	1.006	1.005

TABLE VIII. The ratios of the length to velocity gauges (A^L/A^v) for each of the transitions for Sc $K\alpha$ at different levels of expansions in the calculations.

$K\beta$	$4s$	$4f$	$5s$	$5f$	$6s$	$6f$
Diagram	1.028	1.022	1.022	1.015	1.009	1.008
$3s$ Sat.	1.026	1.027	1.021	1.016	1.010	1.008
$3p$ Sat.	1.022	1.022	1.020	1.013	1.006	1.006
$3d$ Sat.	1.027	1.027	1.012	1.009	1.007	1.007
$4s$ Sat.	1.029	1.030	1.028	1.011	1.011	1.010

TABLE IX. The ratios of the length to velocity gauges (A^L/A^v) for each of the transitions for Sc $K\beta$ at different levels of expansions in the calculations.

$K\alpha$	$4f$	$5s$	$5f$	$6s$	$6f$
Diagram	0.993	0.996	0.999	0.999	0.999
$3s$ Sat.	0.992	0.993	0.995	0.998	0.998
$3p$ Sat.	0.994	0.995	0.995	0.999	0.999
$3d$ Sat.	0.988	0.993	0.994	0.996	0.997
$4s$ Sat.	0.994	0.998	0.998	0.998	0.999

TABLE X. The ratios of the amplitude of transition for the velocity gauge (A^v) values between the current energy level and the immediate previous energy level. i.e. $A^v(4f)/A^v(4s)$ etc. These are given for each of the transitions for Sc $K\alpha$.

$K\alpha$	$4f$	$5s$	$5f$	$6s$	$6f$
Diagram	0.993	0.996	0.999	0.999	0.999
$3s$ Sat.	0.992	0.993	0.995	0.998	0.998
$3p$ Sat.	0.994	0.995	0.995	0.999	0.999
$3d$ Sat.	0.988	0.993	0.994	0.996	0.997
$4s$ Sat.	0.994	0.998	0.998	0.998	0.999

TABLE XI. The ratios of the amplitude of transition for the velocity gauge (A^v) values between the current energy level and the immediate previous energy level. i.e. $A^v(4f)/A^v(4s)$ etc. These are given for each of the transitions for Sc $K\beta$.